ARTICLES
PUBLISHED ONLINE: 19 DECEMBER 2010 | DOI: 10.1038/NGEO1040

nature geoscience

Positive feedback and momentum growth during debris-flow entrainment of wet bed sediment

Richard M. Iverson[1]*, Mark E. Reid[2], Matthew Logan[1], Richard G. LaHusen[1], Jonathan W. Godt[3] and Julia P. Griswold[1]

Debris flows typically occur when intense rainfall or snowmelt triggers landslides or extensive erosion on steep, debris-mantled slopes. The flows can then grow dramatically in size and speed as they entrain material from their beds and banks, but the mechanism of this growth is unclear. Indeed, momentum conservation implies that entrainment of static material should retard the motion of the flows if friction remains unchanged. Here we use data from large-scale experiments to assess the entrainment of bed material by debris flows. We find that entrainment is accompanied by increased flow momentum and speed only if large positive pore pressures develop in wet bed sediments as the sediments are overridden by debris flows. The increased pore pressure facilitates progressive scour of the bed, reduces basal friction and instigates positive feedback that causes flow speed, mass and momentum to increase. If dryer bed sediment is entrained, however, the feedback becomes negative and flow momentum declines. We infer that analogous feedbacks could operate in other types of gravity-driven mass flow that interact with erodible beds.

Debris flows are common phenomena in mountainous regions worldwide. They generally begin on slopes >30°, and culminate when surging mixtures of fragmented rock and muddy water disgorge from canyons onto valley floors[1]. Typically including 50–70% solid grains by volume, attaining speeds >10 m s^{-1} and ranging in size up to ~10^9 m^3, debris flows can denude mountainsides, inundate floodplains and devastate people and property[2]. Recent studies indicate that the incidence and impacts of debris flows may grow if landscape exploitation and climate instability increase[3–5].

Debris flows commonly gain much of their mass and destructive power by entraining material as they descend steep slopes and channels[6]. Previous studies have shown that entrainment can result from scour of bed sediment or collapse of stream banks, and can cause debris-flow mass to grow manyfold before deposition begins on flatter terrain downstream[7–16]. Fundamental questions have remained, however, about the mechanics of mass growth and their effect on flow-momentum growth. A lack of data obtained under controlled conditions is partly responsible[17], but evidence from numerical models is also equivocal. Different models yield different results, and even the best models of debris-flow or avalanche interactions with erodible beds include poorly constrained equations or parameter values[18–23]. Bench-top experiments have recently demonstrated that bed-sediment entrainment by dry granular avalanches can, in some cases, be accompanied by increased flow-front speeds and run-out distances[24], but similarly small experiments have limited relevance for water-laden debris flows owing to the scale-dependent properties of wet granular debris[2,25,26].

To minimize scaling problems while maintaining the advantages of a laboratory setting, we conducted entrainment experiments in a uniquely large facility, the USGS debris-flow flume (Fig. 1). The experiments revealed how entrainment of static sediment can result in conspicuous flow-momentum growth. Moreover, they

Figure 1 | Photographs of the USGS debris-flow flume during entrainment experiment A. Flow discharging onto a concrete run-out pad, where a 1 m grid provides scale. Inset, a photo taken about 6 s earlier shows the agitated flow front encountering bed sediment about 20 m downslope from the flume headgate.

[1]US Geological Survey, Vancouver, Washington 98683, USA, [2]US Geological Survey, Menlo Park, California 94025, USA, [3]US Geological Survey, Denver, Colorado 80225, USA. *e-mail: riverson@usgs.gov.

© 2011 Macmillan Publishers Limited. All rights reserved.

provided the first controlled, field-scale tests of two longstanding hypotheses: that rapid loading by debris flows generates high pore-water pressures in wet bed sediment and thereby facilitates entrainment[12,27,28] and that entrainment occurs by mass movement rather than progressive scour of the bed[29].

Momentum conservation during entrainment

The relationship between entrainment and evolution of flow mass and momentum has been the subject of debate[30–32], but the crux of the problem can be seen with the aid of a simple two-body model. Consider a debris flow that initially has mass m_f and downslope velocity v_f interacting with bed material that initially has mass m_b and downslope velocity $v_b = 0$. During entrainment, the change in flow momentum resulting from transfer of a mass Δm from the bed to the flow is $(m_f + \Delta m)(v_f + \Delta v_f) - m_f v_f$, where Δv_f is the attendant change in flow velocity. The accompanying change in bed momentum is $(m_b - \Delta m)\Delta v_b$, where Δv_b is the mean velocity imparted to previously static bed material by the shear traction at the base of the flow. Momentum conservation dictates that the changes in flow and bed momentum add to zero: $v_f \Delta m + m_f \Delta v_f + \Delta m \Delta v_f + m_b \Delta v_b - \Delta m \Delta v_b = 0$. Dividing all terms of this equation by the time increment Δt over which the mass and momentum exchanges occur and taking the limit as $\Delta t \to 0$ reduces the equation to $d(m_f v_f)/dt = -m_b(dv_b/dt)$. Addition of the downslope driving and resisting forces affecting the flow, ΣF_f, and the bed, ΣF_b, then yields the two-body momentum balance

$$\frac{d(m_f v_f)}{dt} = \Sigma F_f + \Sigma F_b - m_b \frac{dv_b}{dt} \qquad (1)$$

Equation (1) demonstrates that evolution of flow momentum $m_f v_f$ depends not only on the rate of momentum transfer to the bed, $m_b(dv_b/dt)$, but also on any attendant modification of ΣF_f and on reaction forces that necessarily modify ΣF_b. In the bed's initial, static state, $\Sigma F_b = 0$ applies, but $\Sigma F_b > 0$ is necessary for some fraction of the bed to move, and bed motion is accompanied by growth of flow momentum only if $\Sigma F_f + \Sigma F_b > m_b(dv_b/dt)$. A more sophisticated analysis that employs a two-layer continuum model of momentum exchange leads to the same inference (see Supplementary Information).

Equation (1) is too simplistic to yield accurate quantitative predictions, but it motivates measurements of $\Sigma F_f + \Sigma F_b$ during entrainment. We made non-invasive measurements that exploited the fact that a nearly tabular mass with gradually varying thickness h encompassing a debris flow and underlying bed sediment on a uniform slope obeys

$$\Sigma F_f + \Sigma F_b \approx [\rho g h \sin\alpha - \rho g h(\partial h/\partial x) - \tau]A \qquad (2)$$

where ρ is the depth-averaged bulk density of the mass, g is the magnitude of gravitational acceleration, α is the slope angle, x is the downslope coordinate and τ is the resisting shear traction acting over the area A where a debris flow or bed sediment contacts an immovable substrate[33]. If τ arises from Coulomb friction, as is generally true for cohesionless soils and other granular materials, then the maximum value of τ (which applies during incipient or ongoing deformation) can be modelled as $\tau = \mu(\sigma - p)$, where μ is a friction coefficient, σ is the total normal traction on A and p is basal pore-fluid pressure, which can partially or completely counteract σ (ref. 34). A chief goal of our experiments was to control or measure the quantities σ, p, h, ρ, μ and α that affect $\Sigma F_f + \Sigma F_b$ during debris-flow interaction with bed sediment, and simultaneously to evaluate changes in flow mass and momentum.

Entrainment experiments

In a 95-m-long, 2-m-wide flume, we carried out eight experiments (A–H) in which water-saturated, 6-m^3 debris flows

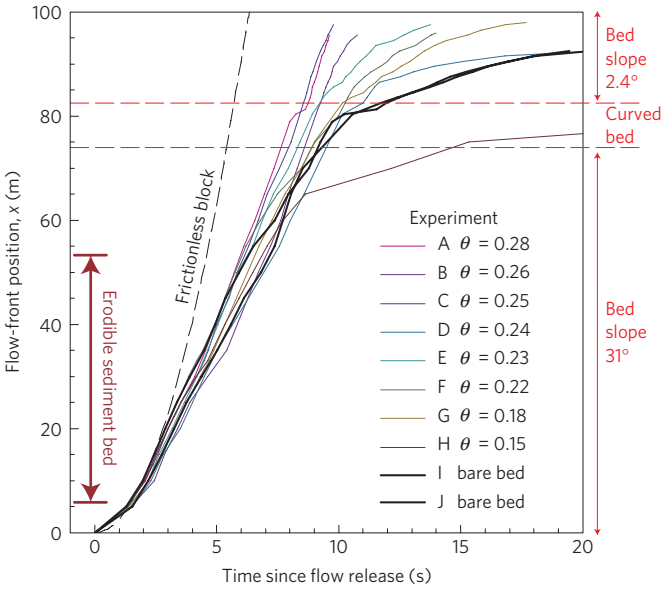

Figure 2 | Measured positions of debris-flow fronts in experiments A–J as a function of time and bed-sediment volumetric water content, θ. Black lines depict data from control experiments I and J. The dashed reference line depicts the theoretical behaviour of a frictionless block.

containing about 56% gravel, 37% sand and 7% mud-sized grains (a thoroughly characterized mixture we call 'SGM' (ref. 26)) discharged abruptly from a headgate and flowed across beds of partially saturated SGM (Supplementary Fig. S1). The nearly tabular sediment beds averaged 12 cm in thickness and covered the uniformly sloping ($\alpha = 31°$) flume bed from $x = 6$ to 53 m, where $x = 0$ denotes the headgate location (see Methods and Supplementary Table S1). We also carried out two control experiments (I and J) with 6-m^3 SGM debris flows but no bed sediment.

The key variable we manipulated was the bed-sediment volumetric water content, θ. Samples of the SGM lining the flume initially had porosities of 0.45 ± 0.04 and volumetric water contents of 0.15 ± 0.02, but after sampling we gradually increased θ by watering the sediment using a system of overhead sprinklers. In this way we created beds with θ ranging from 0.15 ± 0.03 to 0.28 ± 0.04 before debris-flow release (see Methods).

At $x = 32$ and 66 m we deployed arrays of electronic sensors to make 500 Hz measurements of σ, p and h (Supplementary Fig. S1). At $x = 32$ m the sensors detected both the bed sediment and passing debris flows, but at $x = 66$ m they detected post-entrainment flows moving across the bare concrete bed. Details of sensor properties, calibrations, measurement uncertainties and data-processing techniques are presented elsewhere[26].

At several locations from $x = 13$ to 43 m we also recorded 500 Hz data from four to 16 scour sensors installed in the bed sediment (Supplementary Fig. S1). These sensors consisted of artificial gravel clasts, buried at depths of 2–10 cm, which were tethered to electronic circuits by weak contact switches. Breakage of the contacts signalled the timing of clast entrainment.

As proxies for gauging the mass and momentum of debris flows after they entrained sediment but before they encountered slopes <31° at the foot of the flume, we used flow volumes and flow-front speeds measured from $x = 60$ to 70 m (Supplementary Fig. S1). We obtained post-entrainment flow volumes by measuring bed-sediment volumes before and after passage of debris flows and adding the difference to the initial 6-m^3 flow volume, and we measured flow-front speeds on time-stamped video recordings (see Methods). The video recordings, which are viewable online and indexed by experiment

© 2011 Macmillan Publishers Limited. All rights reserved.

date (Supplementary Table S1), constitute an important part of our experiment documentation[35].

Measured mass and momentum changes

Following sudden opening of the flume headgate, debris-flow fronts accelerated nearly like frictionless blocks as they travelled to $x \approx 20$ m (Figs 1 and 2). These large accelerations resulted from the 'dam-break' initial condition and strong longitudinal thrust (represented by $-\rho g h(\partial h/\partial x)$ in equation (2)) imparted during collapse of the impounded debris. As a consequence, all debris flows thinned and elongated at similar rates during the first 2–3 s of motion.

After about 3 s the effects of bed sediment on flow behaviour became conspicuous (Figs 1 and 2). Flow-front accelerations universally diminished, but flows that encountered the wettest bed sediment (A–C) seemed to behave almost explosively as their depths and agitation grew rapidly[35]. By contrast, flows that encountered the driest beds (G and H) seemed much like the flows in bare-bed control experiments (I and J).

After flow fronts moved beyond the sediment beds, their normalized speeds (defined as $S =$ measured speed/9.8 m s^{-1} (the mean speed at $x = 60$–70 m in bare-bed control experiments)) generally increased with θ but surpassed one only if $\theta \geq 0.24$ (Fig. 3a). These flow-front speeds provided suitable proxies for overall flow speeds because sensor data indicated that $h(t)$ waveforms evolved only moderately between $x = 32$ and 66 m (see, for example, Fig. 4a,b). Therefore, flow was almost uniformly progressive[36] over this distance.

Flows that interacted with wet bed sediment also entrained more material and exhibited longer run-outs than flows that interacted with dryer beds. Normalized post-entrainment flow volumes (defined as $V =$ total volume/6 m^3 (the flow volume in control experiments)) exceeded one in every case and increased systematically with θ (Fig. 3b). Even some flows that lost significant speed during entrainment (F and G) exhibited run-out distances that exceeded those of the bare-bed control flows (Supplementary Table S1). Thus, enhanced run-out by itself was not a clear indicator of momentum gains.

To characterize the net effect of entrainment on flow momentum, we use a normalized momentum gain factor defined as $\Gamma = VS$, such that $\Gamma > 1$ denotes a momentum gain and $\Gamma < 1$ denotes a momentum loss relative to the reference state measured in control experiments. Data from experiments with $\theta \geq 0.23$ consistently yield $\Gamma > 2$, whereas those with $\theta \leq 0.22$ yield Γ close to or less than one (Fig. 3c). In the experiments with the wettest beds (A and B), flow momentum nearly quadrupled ($\Gamma \approx 4$) as a consequence of interaction with bed sediment.

A comparison of detailed sensor data recorded in representative experiments with relatively wet and dry beds (C with $\theta = 0.25$ and G with $\theta = 0.18$) reveals the mechanism by which θ influenced mass and momentum change (Fig. 4). The black traces in Fig. 4a–f depict $h(t), \sigma(t)$ and $p(t)$ measured as the two flows interacted with bed sediment at $x = 32$ m, and the red traces depict analogous data acquired at $x = 66$ m, downslope of the erodible beds. These data show that flow C was both deeper and faster than flow G at $x = 66$ m, but that each flow exhibited behaviour typical of debris flows in the laboratory and field[2,26,37,38]: each flow had an abrupt front arrival, followed soon by increases in σ and p. Within 1–2 s σ and p became more or less proportional to each other and to h, and this pattern persisted in the trailing flow. By contrast, at $x = 32$ m, p increased minimally as flow G passed over relatively dry bed sediment (Fig. 4f), whereas the wetter bed sediment in flow C exhibited an increase in p commensurate with the increase in σ (Fig. 4e).

The disparity in bed-sediment pore-pressure responses in experiments C and G was accompanied by large differences in entrainment (Fig. 4i,j). In experiment C scour sensors at 2 cm depth first detected entrainment about 1 s after the flow front passed, implying that rapid erosion commenced as pore pressures increased. Erosion then proceeded downward into the sediment at 5–10 cm s^{-1} at all locations where measurements were made. Thus, the data indicated that spatially uniform, rapid scour occurred, but not mass movement of the bed. In experiment G, by contrast, scour into the relatively dry bed sediment never penetrated to depths where it was detected by sensors.

To estimate the evolving local forces affecting momentum change during entrainment, we combined equation (2) with the

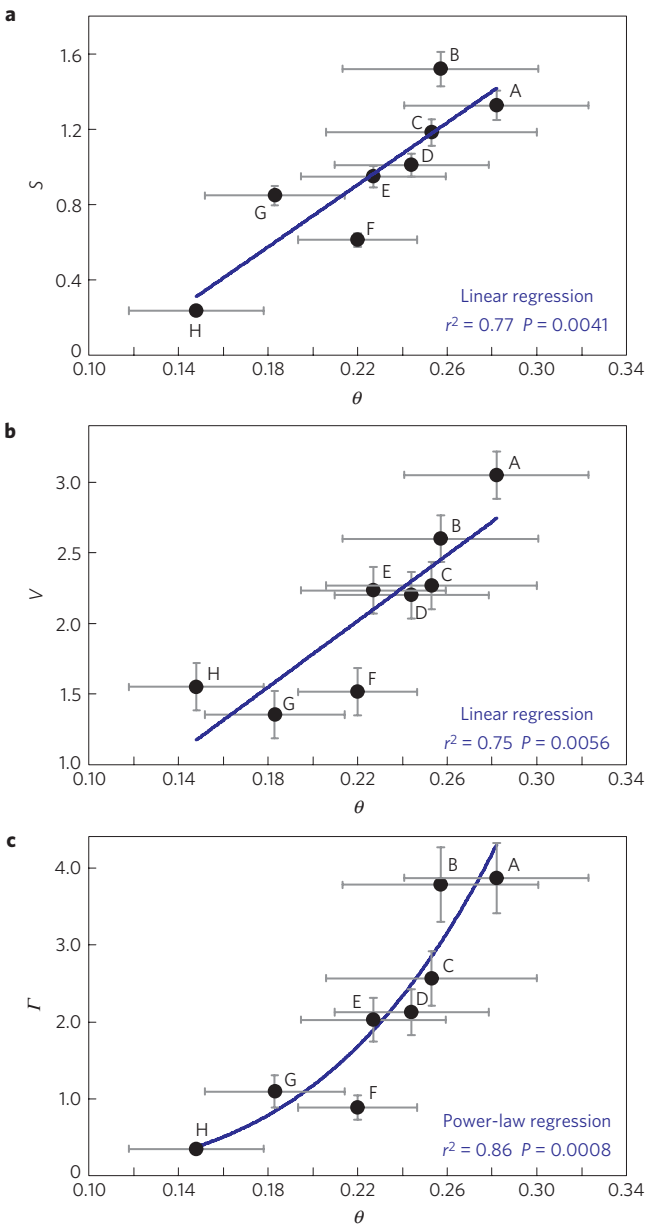

Figure 3 | Post-entrainment flow conditions as a function of bed water content θ in experiments A–H. a, Normalized flow-front speeds, S; **b**, normalized flow volumes, V; **c**, normalized momentum gains, Γ, gauged at $x = 60$–70 m. Data are normalized using reference values measured in control experiments I and J. Error bars for θ express standard deviations of 15–20 spatially distributed measurements, and error bars for S, V and Γ express cumulative measurement uncertainties, as detailed in Methods. Blue lines, r^2 values and P values summarize results of two-parameter least-squares regressions.

© 2011 Macmillan Publishers Limited. All rights reserved.

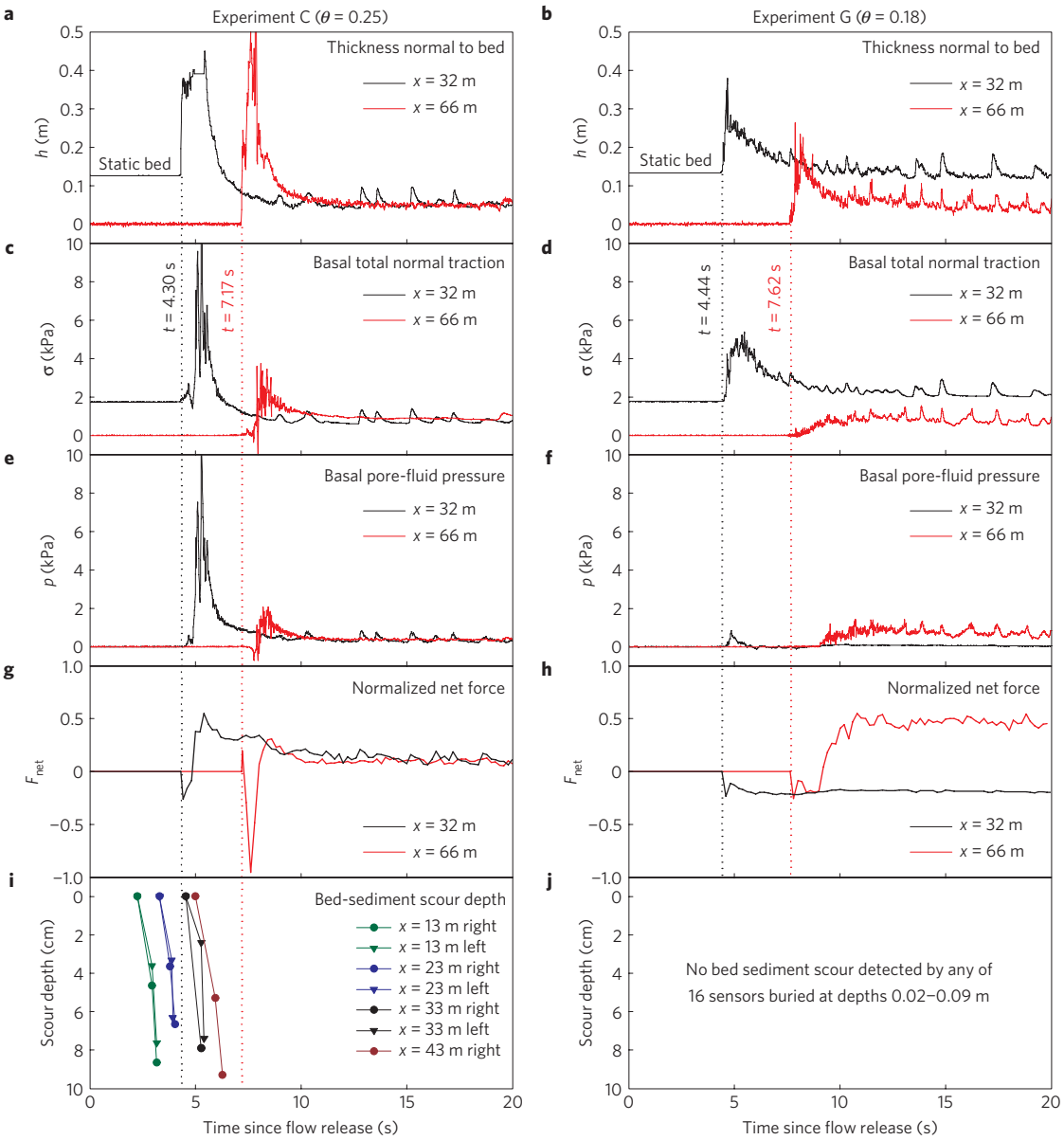

Figure 4 | Time-series data acquired at $x = 32$ and 66 m in two experiments (C and G) with contrasting bed-sediment water contents (θ). a–f, Sensor measurements of flow thickness, $h(t)$, basal total normal traction, $\sigma(t)$, and basal pore-fluid pressure, $p(t)$. **g,h**, Values of F_{net} computed from $h(t)$, $\sigma(t)$ and $p(t)$ and the mean friction coefficient $\mu = 0.84$ measured for SGM (ref. 26). **i,j**, Timing of scour of artificial gravel clasts buried at various depths and distances (x) downslope.

estimates $\rho = \sigma/gh\cos\alpha$ and $\tau = \mu(\sigma - p)$ to obtain an expression for the net normalized force per unit basal area, F_{net}:

$$F_{net} = \frac{\Sigma F_f + \Sigma F_b}{\rho g h A} = \sin\alpha - \cos\alpha \frac{\mu(\sigma - p)}{\sigma} - \frac{\partial h}{\partial x} \qquad (3)$$

We evaluated this formula by first smoothing the time-series data in Fig. 4a–f using a running-median technique and then using a finite-difference approximation of $\partial h/\partial x$, as detailed elsewhere[26]. Results of this procedure are shown in Fig. 4g,h, where $F_{net} > 0$ indicates that force acted locally to accelerate the flow, $F_{net} < 0$ indicates a decelerating force and $F_{net} = \sin\alpha = 0.515$ characterizes fully liquefied flow with $\partial h/\partial x = 0$.

The values of F_{net} in Fig. 4 demonstrate that differences in the momentum gained by flows C and G did not result merely from drying or wetting of the flows as they acquired bed sediment. Indeed, at $x = 66$ m, all but the head of flow G had a large F_{net} (~ 0.5) because the flow entrained little of the relatively dry bed sediment it encountered upslope (Fig. 3b). Flow C, by contrast, entrained most of the unsaturated bed sediment upslope, causing the flow to dry somewhat before it reached $x = 66$ m, and producing an average F_{net} smaller than that in flow G. Nevertheless, flow C gained considerable momentum as a result of entrainment, whereas flow G gained essentially none (Fig. 3c).

Differences in momentum gains by flows C and G are explained by the very different behaviours measured beneath the bed sediment at $x = 32$ m. When flow C began to deform the bed sediment, p rose to levels almost sufficient to liquefy the bed (Fig. 4c,e). As a result, $F_{net} > 0$ developed shortly after passage of the flow front, and persisted as most of the bed material mobilized and became entrained in the flow (Fig. 4g). Although momentum was necessarily transferred out of the flow and into the deforming bed during this process, the flow gained momentum because basal friction was reduced almost to zero as the flow thickened, and

© 2011 Macmillan Publishers Limited. All rights reserved.

the increasing magnitude of $h(\partial h/\partial x)$ at the head of the flow helped drive it downslope. In flow G, on the other hand, $F_{net} < 0$ persisted during flow interaction with the relatively dry sediment bed (Fig. 4h), and little momentum was transferred to the bed as a thin flow rode over the top.

Processes and implications of pore-pressure development

Our experimental results show that pore pressures generated as wet bed sediment is overridden and progressively entrained by debris flows can reduce friction and lead to pronounced flow-momentum growth. Friction reduction does not occur immediately beneath dilated flow fronts, but instead follows front arrival by about 1 s. This lag causes flow fronts to steepen and deepen, accentuating classic debris-flow behaviour in which bulbous fronts advance downslope partly by virtue of their own steepness and partly in response to being pushed by low-friction trailing debris[2,26,39,40].

The conspicuous effect of bed-sediment water content and pore-pressure responses on growth of debris-flow mass and momentum prompts questions about the mechanism of pore-pressure change. In all of our experiments bed-sediment water contents were smaller than those required for complete saturation of the settled sediment (that is, $\theta \approx 0.4$). Nevertheless, provided that $\theta > 0.22$, pore pressures increased from ~0 to nearly lithostatic values in about 1 s when the sediment was overridden by debris flows. In such circumstances pore water was probably interconnected and capable of pressure transmission, whereas most air bubbles in pores were probably entrapped by surrounding water. With $\theta < 0.22$, bed-sediment pore-pressure responses during debris-flow loading were much smaller, apparently because discontinuity of pore water enabled compressed air to escape too easily to sustain large pressure changes.

Direct compression of pores by debris-flow weight was probably only partly responsible for pore-pressure changes in bed sediment, however. Our scour-sensor data imply that shear deformation of the bed occurred concurrently with pore-pressure increases (for example Fig. 4i). Thus, the loose state of the bed sediment probably caused it to contract during the initial stages of shearing, analogous to contraction that occurs when debris flows initiate from loosely packed landslides[41–43]. This shear-induced contraction can increase pore pressures rapidly, even if loading by superincumbent weight is modest.

Our finding that pore-pressure generation in wet bed sediment causes synergistic growth of debris-flow mass and momentum does not preclude the possibility that pore-pressure generation in dry beds could have similar effects in some circumstances. Researchers have speculated that snow avalanches may produce high pore-air pressures as they override and entrain snow beds; see, for example, ref. 20. Small-scale experiments have recently revealed that granular flows entraining dry bed sediment can exhibit enhanced speeds and run-outs, especially if the sediment beds are thick and steep[24], and other experiments have demonstrated that dry grain flows can produce increased basal pore-air pressures as they move across rigid beds[44]. The possibility that air pressure or other phenomena may contribute to friction reduction during entrainment does not diminish the significance of bed sediment wetness, however. Wet beds are typical of debris-flow paths, and our experiments establish a clear link between bed wetness and positive feedback that leads to flow mass and momentum growth.

Methods

In each of our ten experiments the 31° concrete flume bed from $x = 6$ to 74 m was surfaced with bumps that caused the static basal friction coefficient of SGM to match its internal friction coefficient: $\mu = 0.84 \pm 0.08$ (which indicates an angle of repose ≈40°; ref. 26). As a result, bed sediments did not shear preferentially along the concrete surface as they were deformed by debris flows.

Details of our SGM properties, debris-flow release protocols and sediment sampling and measurement techniques are described elsewhere[26], but some procedures specific to our preparation and measurement of sediment beds require explanation. We formed each bed by sliding ~0.3 m^3 loads of moist SGM down the flume along a retractable plastic sheet and then using rakes to redistribute the sediment into a tabular layer. This process involved some disturbance but no net compaction; it produced bed-sediment porosities that differed negligibly from those of the SGM loaded behind the headgate: 0.45 ± 0.04. (Here, and elsewhere in this paper, '±' denotes one standard deviation from the mean of multiple measurements of sediment properties.) Bed-sediment porosity reductions to values ~ 0.4 seemed likely on the basis of settlements we observed during wetting, but a propensity for instability of the wet beds prevented us from resampling the sediment after sprinkling was completed. Indeed, in some experiments small regions of bed sediment on the 31° slope failed spontaneously during wetting, despite our efforts to avoid producing regions of complete saturation and positive pore-water pressure. During bed-sediment wetting we measured pore-water pressures by using tensiometers fitted with pressure transducers and measured θ by using 15–20 spatially distributed high-frequency electrical capacitance sensors (Decagon Devices model ECH_20 EC-5), which indirectly gauged dielectric permittivity, a property that is related to sediment water content through empirical calibrations[45]. (Our use of trade, product or firm names is for descriptive purposes only and does not imply endorsement by the US Government.)

We measured bed-sediment thicknesses before and after passage of debris flows by using either graduated surface-contact probes or, later, a laser ranging device. At a minimum, we measured thicknesses at intervals of 0.2 m in the cross-flume direction and 2.5 m in the down-flume direction, with a bed-normal resolution of 5 mm. We used these measurements to create isopach maps of sediment thicknesses, and we differenced preflow and postflow maps to determine the distribution and volume of net bed erosion. Several sources may have contributed to error in this process, but an error budget and empirical tests indicated that the cumulative error was probably < 1 m^3, and we used this value to determine error bars for V in Fig. 3b. We determined error bars for S in Fig. 3a by using the 0.03 s resolution of time-stamped video recordings to estimate a maximum cumulative error of 0.06 s in flow-front transit time from $x = 60$ to 70 m. We determined error bars for Γ in Fig. 3c by propagating the errors in S and V.

Received 8 July 2010; accepted 19 November 2010; published online 19 December 2010

References

1. Takahashi, T. *Debris Flow—Mechanics, Prediction and Countermeasures* (Taylor & Francis, 2007).
2. Iverson, R. M. The physics of debris flows. *Rev. Geophys.* **35,** 245–296 (1997).
3. Pierce, J. L., Meyer, G. A. & Jull, A. J. T. Fire-induced erosion and millennial-scale climate change in northern ponderosa pine forests. *Nature* **432,** 87–90 (2004).
4. Stoffel, M. & Beniston, M. On the incidence of debris flows from the early Little Ice Age to a future greenhouse climate: A case study from the Swiss Alps. *Geophys. Res. Lett.* **33,** L16404 (2006).
5. Jakob, M. & Friele, P. Frequency and magnitude of debris flows on Cheekye River, British Columbia. *Geomorphology* **114,** 382–395 (2009).
6. Hungr, O., McDougall, S. & Bovis, M. in *Debris-Flow Hazards and Related Phenomena* (eds Jakob, M. & Hungr, O.) 135–158 (Springer, 2005).
7. Benda, L. The influence of debris flows on channels and valley floors in the Oregon Coast Range, USA. *Earth Surf. Proc. Landf.* **15,** 457–466 (1990).
8. Pierson, T. C., Janda, R. J., Thouret, J-C. & Borrero, C. A. Perturbation and melting of snow and ice by the 13 November 1985 eruption of Nevado del Ruiz, Colombia, and consequent mobilization, flow and deposition of lahars. *J. Volcanol. Geotherm. Res.* **41,** 17–66 (1990).
9. Berti, M., Genevois, R., Simoni, A. & Rosella Tecca, P. Field observations of a debris flow event in the Dolomites. *Geomorphology* **29,** 265–274 (1999).
10. Fannin, R. J. & Wise, M. P. An empirical–statistical model for debris flow travel distance. *Can. Geotech. J.* **38,** 982–994 (2001).
11. Rickenmann, D., Weber, D. & Stepanov, B. in *Debris-flow Hazards Mitigation: Mechanics, Prediction, and Assessment,* Vol. 2 (eds Rickenmann, D. & Chen, C-L.) 883–894 (Millpress, 2003).
12. Wang, G., Sassa, K. & Fukuoka, H. Downslope volume enlargement of a debris slide–debris flow in the 1999 Hiroshima, Japan, rainstorm. *Eng. Geol.* **69,** 309–330 (2003).
13. Godt, J. W. & Coe, J. A. Alpine debris flows triggered by a 28 July 1999 thunderstorm in the central Front Range, Colorado. *Geomorphology* **84,** 80–97 (2007).
14. Breien, H., De Blasio, F. V., Elverhøi, A & Høeg, K. Erosion and morphology of a debris flow caused by a glacial lake outburst flood, western Norway. *Landslides* **5,** 271–280 (2008).
15. Berger, C., McArdell, B. W., Fritschi, B. & Schlunegger, F. A novel method for measuring the timing of bed erosion during debris flows and floods. *Water Res.* **46,** W02502 (2010).
16. Guthrie, R. H. *et al.* An examination of controls on debris flow mobility: Evidence from coastal British Columbia. *Geomorphology* **114,** 601–613 (2010).

© 2011 Macmillan Publishers Limited. All rights reserved.

17. Hungr, O., Morgan, G. C. & Kellerhalls, R. Quantitative analysis of debris torrent hazards for design of remedial measures. *Can. Geotech. J.* **21,** 663–677 (1984).
18. Pouliquen, O. & Foreterre, Y. Friction law for dense granular flows: Application to the motion of a mass down a rough inclined plane. *J. Fluid Mech.* **453,** 133–151 (2002).
19. Chen, H., Crosta, G. B. & Lee, C. F. Erosional effects on runout of fast landslides, debris flows and avalanches: A numerical investigation. *Geotechnique* **56,** 305–322 (2006).
20. Sovilla, B., Burlando, P. & Bartelt, P. Field experiments and numerical modelling of mass entrainment in snow avalanches. *J. Geophys. Res.* **111,** F03007 (2006).
21. Mangeney, A., Tsimring, L. S., Volfson, D., Aranson, I. S. & Bouchut, F. Avalanche mobility induced by the presence of an erodible bed and associated entrainment. *Geophys. Res. Lett.* **34,** L22401 (2007).
22. Armanini, A., Fraccarollo, L. & Rosatti, G. Two-dimensional simulation of debris flows in erodible channels. *Comput. Geosci.* **35,** 993–1006 (2009).
23. Crosta, G. B., Imposimato, S. & Roddeman, D. Numerical modelling of 2-D granular step collapse on erodible and nonerodible surface. *J. Geophys. Res.* **114,** F03020 (2009).
24. Mangeney, A. *et al.* Erosion and mobility in granular collapse over sloping beds. *J. Geophys. Res.* **115,** F03040 (2010).
25. Bowman, E. T., Imre, B., Laue, J. & Springman, S. M. in *Debris-flow Hazards Mitigation: Mechanics, Prediction, and Assessment,* Vol. 2 (eds Chen, C-L. & Major, J. J.) 229–239 (Millpress, 2007).
26. Iverson, R. M., Logan, M., LaHusen, R. G. & Berti, M. The perfect debris flow? Aggregated results from 28 large-scale experiments. *J. Geophys. Res.* **115,** F03005 (2010).
27. Hutchinson, J. N. & Bhandari, R. K. Undrained loading, a fundamental mechanism of mudflows and other mass movements. *Geotechnique* **21,** 353–358 (1971).
28. Sassa, K., Kaibori, M. & Kitera, N. in *Proc. Int. Symp. on Erosion, Debris Flows and Disaster Prevention* (ed. Takei, A.) 231–236 (The Erosion-control Engineering Society, 1985).
29. Takahashi, T. Mechanical characteristics of debris flow. *J. Hydraul. Division, ASCE* **104,** 1153–1169 (1978).
30. Hungr, O. Momentum transfer and friction in the debris of rock avalanches: Discussion. *Can. Geotech. J.* **27,** 697 (1990).
31. Van Gassen, W. & Cruden, D. M. Momentum transfer and friction in the debris of rock avalanches: Reply. *Can. Geotech. J.* **27,** 698–699 (1990).
32. Erlichson, H. A mass-change model for the estimation of debris-flow runout, a second discussion: Conditions for the application of the rocket equation. *J. Geol.* **99,** 633–634 (1991).
33. Iverson, R. M. & Denlinger, R. P. Flow of variably fluidized granular masses across three-dimensional terrain: 1. Coulomb mixture theory. *J. Geophys. Res.* **106,** 537–552 (2001).
34. Iverson, R. M. & Vallance, J. W. New views of granular mass flows. *Geology* **29,** 115–118 (2001).
35. Logan, M. & Iverson, R. M. *Video Documentation of Experiments at the USGS Debris-flow Flume, 1992–2009.* US Geological Survey Open-file Report 2007-1315, version 2.0 (2007) http://pubs.usgs.gov/of/2007/1315/.
36. Hungr, O. Analysis of debris flow surges using the theory of uniformly progressive flow. *Earth Surf. Process Landf.* **25,** 483–495 (2000).
37. McArdell, B. W., Bartelt, P. & Kowaslski, J. Field observations of basal forces and fluid pore pressure in a debris flow. *Geophys. Res. Lett.* **34,** L07406 (2007).
38. McCoy, S. W. *et al.* Evolution of a natural debris flow: *In situ* measurements of flow dynamics, video imagery, and terrestrial laser scanning. *Geology* **38,** 735–738 (2010).
39. Sharp, R. P. & Nobles, L. H. Mudflow of 1941 at Wrightwood, southern California. *Geol. Soc. Am. Bull.* **64,** 547–560 (1953).
40. Pierson, T. C. in *Hillslope Processes* (ed. Abrahams, A. D.) 269–296 (Allen & Unwin, 1986).
41. Iverson, R. M., Reid, M. E. & LaHusen, R. G. Debris-flow mobilization from landslides. *Annu. Rev. Earth Planet. Sci.* **25,** 85–138 (1997).
42. Iverson, R. M. *et al.* Acute sensitivity of landslide rates to initial soil porosity. *Science* **290,** 513–516 (2000).
43. Iverson, R. M. Regulation of landslide motion by dilatancy and pore-pressure feedback. *J. Geophys. Res.* **110,** F02015 (2005).
44. Roche, O., Montserrat, S., Niño, Y. & Tamburrino, A. Pore fluid pressure and internal kinematics of gravitational laboratory air-particle flows: Insights into the emplacement dynamics of pyroclastic flows. *J. Geophys. Res.* **115,** B09206 (2010).
45. Kizito, F. *et al.* Frequency, electrical conductivity and temperature analysis of a low-cost capacitance soil moisture sensor. *J. Hydrol.* **352,** 367–378 (2008).

Acknowledgements

We thank K. Swinford, R. Denlinger, S. Henderson, D. George, C. Fox-Lent, J. Coe, W. Schulz, B. McArdell and C. Berger for assisting with experiments, and we thank A. Mangeney, J. Kean and J. Walder for providing useful comments on the manuscript.

Author contributions

R.M.I., M.E.R., M.L., R.G.L. and J.W.G. designed and implemented various facets of the experiments and measurement protocols, and R.M.I., M.E.R., M.L., R.G.L. and J.P.G. collected, processed and analysed the data. R.M.I. wrote the paper, but all authors concurred with the paper's content.

Additional information

The authors declare no competing financial interests. Supplementary information accompanies this paper on www.nature.com/naturegeoscience. Reprints and permissions information is available online at http://npg.nature.com/reprintsandpermissions. Correspondence and requests for materials should be addressed to R.I.

© 2011 Macmillan Publishers Limited. All rights reserved.